doi:10.1093/brain/awz164 BRAIN 2019: 142; 2417–2431 | 2417

BRAIN
A JOURNAL OF NEUROLOGY

# Deep brain stimulation has state-dependent effects on motor connectivity in Parkinson's disease

**Joshua Kahan,[1] Laura Mancini,[2,3] Guillaume Flandin,[4] Mark White,[2,3] Anastasia Papadaki,[2,3] John Thornton,[2,3] Tarek Yousry,[2,3] Ludvic Zrinzo,[1] Marwan Hariz,[1] Patricia Limousin,[1] Karl Friston[4] and Tom Foltynie[1]**

Subthalamic nucleus deep brain stimulation is an effective treatment for advanced Parkinson's disease; however, its therapeutic mechanism is unclear. Previous modelling of functional MRI data has suggested that deep brain stimulation has modulatory effects on a number of basal ganglia pathways. This work uses an enhanced data collection protocol to collect rare functional MRI data in patients with subthalamic nucleus deep brain stimulation. Eleven patients with Parkinson's disease and subthalamic nucleus deep brain stimulation underwent functional MRI at rest and during a movement task; once with active deep brain stimulation, and once with deep brain stimulation switched off. Dynamic causal modelling and Bayesian model selection were first used to compare a series of plausible biophysical models of the cortico-basal ganglia circuit that could explain the functional MRI activity at rest in an attempt to reproduce and extend the findings from our previous work. General linear modelling of the movement task functional MRI data revealed deep brain stimulation-associated signal increases in the primary motor and cerebellar cortices. Given the significance of the cerebellum in voluntary movement, we then built a more complete model of the motor system by including cerebellar-basal ganglia interactions, and compared the modulatory effects deep brain stimulation had on different circuit components during the movement task and again using the resting state data. Consistent with previous results from our independent cohort, model comparison found that the rest data were best explained by deep brain stimulation-induced increased (effective) connectivity of the cortico-striatal, thalamo-cortical and direct pathway and reduced coupling of subthalamic nucleus afferent and efferent connections. No changes in cerebellar connectivity were identified at rest. In contrast, during the movement task, there was functional recruitment of subcortical-cerebellar pathways, which were additionally modulated by deep brain stimulation, as well as modulation of local (intrinsic) cortical and cerebellar circuits. This work provides *in vivo* evidence for the modulatory effects of subthalamic nucleus deep brain stimulation on effective connectivity within the cortico-basal ganglia loops at rest, as well as further modulations in the cortico-cerebellar motor system during voluntary movement. We propose that deep brain stimulation has both behaviour-independent effects on basal ganglia connectivity, as well as behaviour-dependent modulatory effects.

1 Department of Clinical and Movement Neurosciences, UCL Queen Square Institute of Neurology, London, WC1N 3BG, UK
2 Lysholm Department of Neuroradiology, National Hospital for Neurology and Neurosurgery, UCLH NHS Foundation Trust, London, WC1N 3BG, UK
3 Department of Brain Repair and Rehabilitation, UCL Queen Square Institute of Neurology, London, WC1N 3BG, UK
4 The Wellcome Centre for Human Neuroimaging, UCL, London, WC1N 3AR, UK

Correspondence to: Professor Tom Foltynie
Department of Clinical and Movement Neurosciences (Box 146), UCL Queen Square
Institute of Neurology, London, WC1N 3BG, UK
E-mail: t.foltynie@ucl.ac.uk

Received December 11, 2018. Revised March 12, 2019. Accepted April 18, 2019. Advance Access publication June 20, 2019

**Keywords:** Parkinson's disease; deep brain stimulation; functional MRI; connectivity; basal ganglia

**Abbreviations:** BMS = Bayesian model selection; BOLD = blood oxygen level-dependent; DBS = deep brain stimulation; DCM = dynamic causal modelling; GLM = general linear model; STN = subthalamic nucleus; UPDRS = Unified Parkinson's Disease Rating Scale

# Introduction

Deep brain stimulation (DBS) of the subthalamic nucleus (STN) has become an established treatment for some patients with Parkinson's disease (Limousin *et al.*, 1995, 1998; Deuschl *et al.*, 2006). Trials of DBS to treat other neurological and psychiatric diseases are under investigation, leading many to question its mechanism of action so as to maximize its utility (Laxton *et al.*, 2010; Holtzheimer and Mayberg, 2011; Gratwicke *et al.*, 2013). Clinically, DBS can mimic the effect of an ablative lesion, leading many to suggest that DBS 'inhibits activity' in the same way; a theory appealing to firing rate-based models of basal ganglia circuitry (Albin *et al.*, 1989; DeLong, 1990; Beurrier *et al.*, 2001; Meissner *et al.*, 2005). However, both animal and computational models suggest that stimulation has a myriad of effects on different neuronal elements (Perlmutter and Mink, 2006; Deniau *et al.*, 2010; McIntyre and Hahn, 2010; Vedam-Mai *et al.*, 2012), including frequency-dependent reductions in STN firing rates (Beurrier *et al.*, 2001; Welter *et al.*, 2004; Meissner *et al.*, 2005), normalization of cortical phase-amplitude coupling (de Hemptinne *et al.*, 2013, 2015), and both inhibition and excitation of downstream targets (Maurice *et al.*, 2003). Human electrophysiology has similarly revealed reductions in STN beta power (Kühn *et al.*, 2008; Eusebio *et al.*, 2011), and both neuroimaging and EEG have demonstrated altered activity at the level of the cortex (Limousin *et al.*, 1997; Ceballos-Baumann *et al.*, 1999; Boertien *et al.*, 2011; Li *et al.*, 2012), suggesting that neuromodulatory effects, whether direct or indirect, are not limited to the target nucleus.

We have previously identified DBS-related changes in cortico-basal ganglia 'effective' connectivity; i.e. changes in the way regions within the cortico-basal ganglia network impact on one another. Specifically, modelling of the blood oxygen level-dependent signal (BOLD) revealed stimulation-related decreases in STN afferent (both hyperdirect and indirect) and efferent coupling, as well as increases in cortico-striatal, thalamo-cortical and direct pathway coupling while patients lay at rest (Kahan *et al.*, 2014). In addition, there are reports of DBS-associated increased functional connectivity in the motor cortex and premotor area using eigenvector centrality analysis (Mueller *et al.*, 2013, 2018; Holiga *et al.*, 2015), and PET studies have demonstrated that DBS reduces the expression of pathological patterns of functional connectivity such as the Parkinson's disease covariance or tremor patterns (Asanuma *et al.*, 2006; Wang *et al.*, 2010; Ko *et al.*, 2013).

Functional MRI in DBS patients has been largely avoided because of concerns about the effects of magnetic fields on the implanted DBS circuit. Until now, functional MRI data has been collected exclusively using a single channel head-transmit/receive coil (Jech *et al.*, 2001, 2012, Kahan *et al.*, 2012, 2014). We developed an MRI protocol using body-transmit MRI and a 12-channel receive coil (Kahan *et al.*, 2015), theoretically yielding an improved signal-to-noise ratio, whilst minimizing any magnetic resonance-induced electrode heating to $<1.0^{\circ}$C, in line with international guidelines.

In the current study, we model data from a cohort of Parkinson's disease patients with chronically implanted STN DBS, collected under our improved scanning protocol. We first ask whether we can reproduce previously identified changes in basal ganglia coupling in the resting state. We then use the data collected during a movement task to establish how the basal ganglia integrate with the cerebellum, and how this is impacted by DBS. Finally we repeat this analysis on the resting state data and explore whether there is a difference between DBS-related modulatory effects during the resting state, and during the movement task state.

# Materials and methods

This study was approved by the National Hospital and UCL Institute of Neurology Joint Ethics committee (09/H0716/51). All participants provided written informed consent in accordance with the Declaration of Helsinki.

## Experimental design

We used a cross-sectional, unblinded, randomized, cross-over design to explore the effects of STN DBS on 'resting state' effective connectivity, and voluntary movement-related brain activity and connectivity in patients with Parkinson's disease.

## Patients

Eleven patients (10 males, one female) who met Queen Square Brain Bank criteria for idiopathic Parkinson's disease were recruited (Table 1). Stimulation parameters had been previously optimized to clinical responses. Medication was withdrawn for 10–12 h (overnight) before scanning. Inclusion was limited to those patients who could tolerate lying flat with minimal head tremor, while being both off medication and off stimulation. Unified Parkinson's Disease Rating Scale part III (UPDRS-III) motor scores were recorded both on and off stimulation before scanning. Stimulation settings and system impedances were noted. UPDRS-III subscores were calculated for each patient

**Table 1 Patient information**

| Sub | Age | Hand | Post-op | LED | Left hemibody | | Right hemibody | | Total | |
|---|---|---|---|---|---|---|---|---|---|---|
| | | | | | Off | On | Off | On | Off | On |
| 1 | 60 | Right | 24 | 598.75 | 11 | 5 | 12 | 10 | 38 | 21 |
| 2 | 64 | Right | 22 | 632.00 | 22 | 7 | 18 | 10 | 61 | 29 |
| 3 | 34 | Right | 24 | 1190.00 | 29 | 12 | 24 | 11 | 69 | 30 |
| 4 | 43 | Right | 5 | 825.00 | 11 | 7 | 5 | 1 | 26 | 12 |
| 5 | 50 | Right | 28 | 72.00 | 21 | 11 | 18 | 8 | 55 | 28 |
| 6 | 43 | Right | 7 | 600.00 | 21 | 13 | 16 | 11 | 52 | 31 |
| 7 | 49 | Right | 37 | 882.00 | 26 | 14 | 24 | 15 | 75 | 45 |
| 8 | 52 | Left | 25 | 460.00 | 17 | 2 | 17 | 7 | 45 | 12 |
| 9 | 58 | Right | 12 | 370.00 | 23 | 8 | 19 | 7 | 54 | 22 |
| 10 | 61 | Right | 9 | 1731.75 | 17 | 12 | 14 | 7 | 43 | 25 |
| 11 | 65 | Right | 3 | 948.00 | 10 | 3 | 10 | 2 | 32 | 8 |
| Mean | 53 | | 18 | 755.41 | 19 | 9 | 16 | 8 | 50 | 24 |
| SD | 9.7 | | 11.2 | 443.50 | 6.3 | 4.1 | 5.7 | 4.0 | 15.1 | 10.6 |

Patients had received chronic bilateral STN DBS for at least 3 months. Electrode implantation was performed using stereotactic $T_2$-weighted MRI, for both preoperative targeting and immediate postoperative verification (Foltynie *et al.*, 2011; Zrinzo *et al.*, 2011), ensuring electrode contacts were well-sited within the STN. All patients received bilateral electrodes (Model 3389, Medtronic) and a dual channel pacemaker ('implanted pulse generator', IPG, ActivaPC$^{TM}$, Medtronic) implanted in the left pectoral region. Scanning proceeded with no adverse effects; DBS system impedances were unaffected by scanning, and following administration of medication, patients returned to their pre-scan clinical baseline. All UPDRS-III scores were conducted OFF medication. Right and left hemibody scores do not equal total score because there are additional points for axial signs that are not detailed in this table. LED = daily levodopa equivalent dose; Post-op = months since DBS implantation; SD = standard deviation.

including hemi-body scores (the sum of all lateralized items in the scale, including rigidity, bradykinesia and tremor).

## MRI data acquisition

Onsite tissue-equivalent test-object thermometry experiments confirmed that the specific hardware and MRI sequences used in this study were safe to be used in patients with implanted Medtronic ActivaPC$^{TM}$ DBS systems. Additionally, we confirmed that the MRI environment did not interrupt implanted pulse generator (IPG) function (Kahan *et al.*, 2015). Scanning was performed in a Siemens Avanto 1.5 T MRI scanner using the body-transmit coil and a 12-channel receive-only head coil. This differs from our previous studies using a transmit-receive head coil (Kahan *et al.*, 2012, 2014). The decision to modify our protocol was motivated by theoretical signal-to-noise benefits. The specific absorption ratio (SAR) in the head was limited to $<0.4$ W/kg.

Patients were scanned with their stimulation on and off, the order of which was randomized using a random number generator. Patients received three scans in each stimulation condition in addition to standard localizer and field map scans: (i) anatomical $T_1$; (ii) resting state functional MRI; and (iii) movement task functional MRI (see Supplementary material for sequence parameters). Patients entered the scanner with their DBS on, and were either switched off or maintained on before scanning, resulting in a ~10-min latency between DBS manipulation and undergoing functional MRI. During resting state functional MRI, patients were told to lie in the scanner with their eyes closed and not to fall asleep. The movement task functional MRI was based on a paradigm used previously (Kahan *et al.*, 2012). In brief, patients heard an audio stimulus ('beep') at a random interval (between 1 and 3 s) throughout the session, in addition to audio commands alternating between 'rest' and 'go' every 30 s. During 'go' blocks, patients were instructed to perform a joystick movement with their left hand as fast as possible each time they heard a beep. A movement entailed displacing the handle from the centre in a direction of their choice, and then returning it to the centre. Additionally, patients were instructed to plan their next movement between each beep. During 'rest' blocks, patients were instructed to rest their hand on the joystick and ignore the beeps. Patients were given practice runs before entering the scanner, and were monitored throughout to ensure they were performing the task correctly. There were nine rest and eight movement blocks in each session. The table was then withdrawn from the magnet, keeping the patient's head in the head coil, and their DBS was switched to the opposite condition. Both patient and experimenter were unblinded to the DBS condition due to the magnitude of the treatment effect.

## Processing the functional MRI data

All analyses were performed using Statistical Parametric Mapping (SPM12b; http://www.fil.ion.ucl.ac.uk/spm). The first five scans of each session (one rest and one movement session per stimulation condition per subject = four sessions per subject) were removed and data were corrected for field inhomogeneity using the field maps. Data were then realigned and unwarped to account for any head movements throughout the functional MRI sessions. Imaging data were then coregistered with anatomical scans, segmented, normalized to MNI space, spatially smoothed using a Gaussian kernel (8 mm full-width at half-maximum) and quality controlled by visual inspection.

## Experiment I: Are previously reported effects of STN DBS on resting state connectivity reproducible?

Resting state functional MRI data were initially treated identically to those described in (Kahan *et al.*, 2014), with the exception that only right hemisphere data were analysed.

Data from each DBS condition were concatenated and modelled using a General Linear Model (GLM), composed of (i) a discrete cosine basis set containing functions with frequencies characteristic of resting state fluctuations (0.0078–0.1 Hz); (ii) a regressor encoding the effect of DBS; (iii) six nuisance regressors from each session capturing head motion; and (iv) confound time series from extra-cerebral compartments.

### Preparing the volumes of interest

Functionally-defined M1 coordinates for each subject derived from Experiment II (see below) were used to guide extraction of functionally relevant data from the resting state dataset. The resting state M1 BOLD signal was summarized with the principal eigenvariate (adjusted for confounds: head movements and extra-cerebral compartments) of a sphere (radius 4 mm) of voxels centred on the subject-specific M1 coordinate. Basal ganglia masks were created using probabilistic white matter connectivity atlases (Behrens *et al.*, 2003; Tziortzi *et al.*, 2014), and were used to restrict selection of subcortical voxels to regions of the putamen and thalamus that exhibit strong structural connectivity with M1 at a population level. A psychophysiological interaction (PPI) (Friston *et al.*, 1997) between resting state M1 activity and DBS, masked with images of the putamen and thalamus, was used to define the voxels in the putamen and thalamus to be included in our connectivity analysis. The BOLD data from the putamen and thalamus respectively were extracted centred on the peak T-statistic within each mask, producing three volumes of interest per subject (M1, putamen, thalamus). BOLD data from the STN were not considered because of its small size and loss-of-signal artefact caused by the DBS electrode.

### Dynamic causal modelling

Dynamic causal modelling (DCM) aims to explain observed neuroimaging data in terms of coupling (i.e. effective connectivity) within and between a network of brain regions (Friston *et al.*, 2003). Coupling in DCM is directed, and summarizes the causal effect one region exerts on either itself (intrinsic), or on another region (extrinsic)—known as effective connectivity. This contrasts with functional connectivity, which usually concerns the correlations between two regions. For an introductory overview of DCM, see Kahan and Foltynie (2013).

The volumes of interest were used to construct 32 DCMs (per subject) representing different hypothetical architectures. Two-state (Marreiros *et al.*, 2008) stochastic DCM for functional MRI (Li *et al.*, 2011) was used, endowing each node with excitatory and inhibitory subpopulations in receipt of noisy fluctuating inputs. The STN was modelled as a hidden node, whose noise precision (given the electrode artefact) was effectively zero, forcing the inversion routine to ignore the recorded signal from the node when estimating model parameters. In other words, although a node with the connectivity fingerprint of the STN was included, only BOLD data from the other nodes was used to fit the model (Kahan *et al.*, 2014). Pallidal nodes were not included; rather, their connections were collapsed to simplify the model. Thus, the direct pathway was summarized as an excitatory connection from the putamen to the thalamus, and indirect pathway as an excitatory putamen-STN connection, and an inhibitory STN-thalamus connection. Although there is evidence for polysynaptic connections from the STN to thalamus that could result in excitatory coupling, for simplicity these connections were not modelled. The hyperdirect pathway was defined as the M1-STN connection, and the thalamo-cortical pathway was represented by the connection from the thalamus to M1. The 32 DCMs differed with regards which subset of connections were modulated by active DBS, and are shown graphically in Supplementary Fig. 1. Models were inverted using generalized filtering (Friston *et al.*, 2010; Li *et al.*, 2011), providing an estimate of the coupling parameters and model evidence. The 32 models from each of the 11 patients entered a Bayesian model selection (BMS) procedure (fixed effects assumptions) that compares the free energy of each model, taking into account the model fit and complexity (Stephan *et al.*, 2009; Penny *et al.*, 2010; Rigoux *et al.*, 2013). The model with the highest model evidence was considered the group winner. Winning model coupling parameters from each patient were then compared using two-tailed paired *t*-tests to test for the effects of DBS on specific coupling strengths. Significance was set at $P < 0.05$.

## Experiment II: The effect of STN DBS on voluntary movement-related brain activity and circuit connectivity

### The effects of voluntary movement and DBS on regional BOLD signal

The joystick position data were interrogated and peak velocity ($V_{max}$), reaction time, and randomness of direction choice were calculated (Supplementary material). Preprocessed task functional MRI data were analysed using the standard GLM framework; each subject's task sessions (one per stimulation condition) were entered into a single GLM and blocked stimulus functions were specified in each session coding the effects of voluntary movement. Head position confounds were excluded from first level GLMs due to collinearity with voluntary movement stimulus functions. Stimulus functions were convolved with a canonical haemodynamic response function in the normal way, and the GLMs were then fitted to the data.

Three contrasts were specified: (i) the main effect of movement; (ii) Movement × DBS interaction on > off; (iii) Movement × DBS interaction off > on. The resulting T-maps from each subject were used for second-level (i.e. group) random effects inference. Clusters surviving a threshold of $P < 0.05$ (familywise error corrected for multiple comparisons) at the whole-brain level were considered significant with a voxel intensity threshold of $P < 0.001$ uncorrected.

### Dynamic causal modelling of movement-related BOLD responses

The GLM was rotated for DCM analysis as described previously (Kahan *et al.*, 2014), and volumes of interest were extracted using the Movement × DBS (on > off) contrast and adjusted for confounds, while retaining the effects of interest (i.e. the main effects of movement and DBS, and the Movement × DBS interaction). The regional BOLD signal from each node was summarized with the principal eigenvariate of a sphere of voxels (radius 4 mm) centred on the voxel within each mask demonstrating the largest Movement × DBS interaction. Each structure was masked separately as described in Experiment I. The cerebellar mask was a spherical mask centred on the group maxima taken from the second-level analysis of Movement × DBS interaction.

This produced four volumes of interest per subject (M1, putamen, thalamus, cerebellum; see Supplementary Table 1 for coordinates). Data from the M1, putamen, and thalamus were all contralateral to the limb moved, whereas data from cerebellum was from the midline and ipsilateral to the movement.

The basal ganglia loop was as modelled in Experiment I with additional connections projecting to and from the cerebellar node. The model comparison space posed the following questions: (i) is cerebellar connectivity (DCM A-matrix) best modelled as purely cortico-cerebellar coupling, subcortical-cerebellar coupling, or both; and (ii) is the interaction between movement and DBS best explained by modulatory effects (DCM B-matrix) on cortico-cerebellar coupling, subcortical-cerebellar coupling, intrinsic coupling, or a combination of all three. The main effect of voluntary movement entered all the models as a driving input (DCM C-matrix) into M1 (Fig. 1).

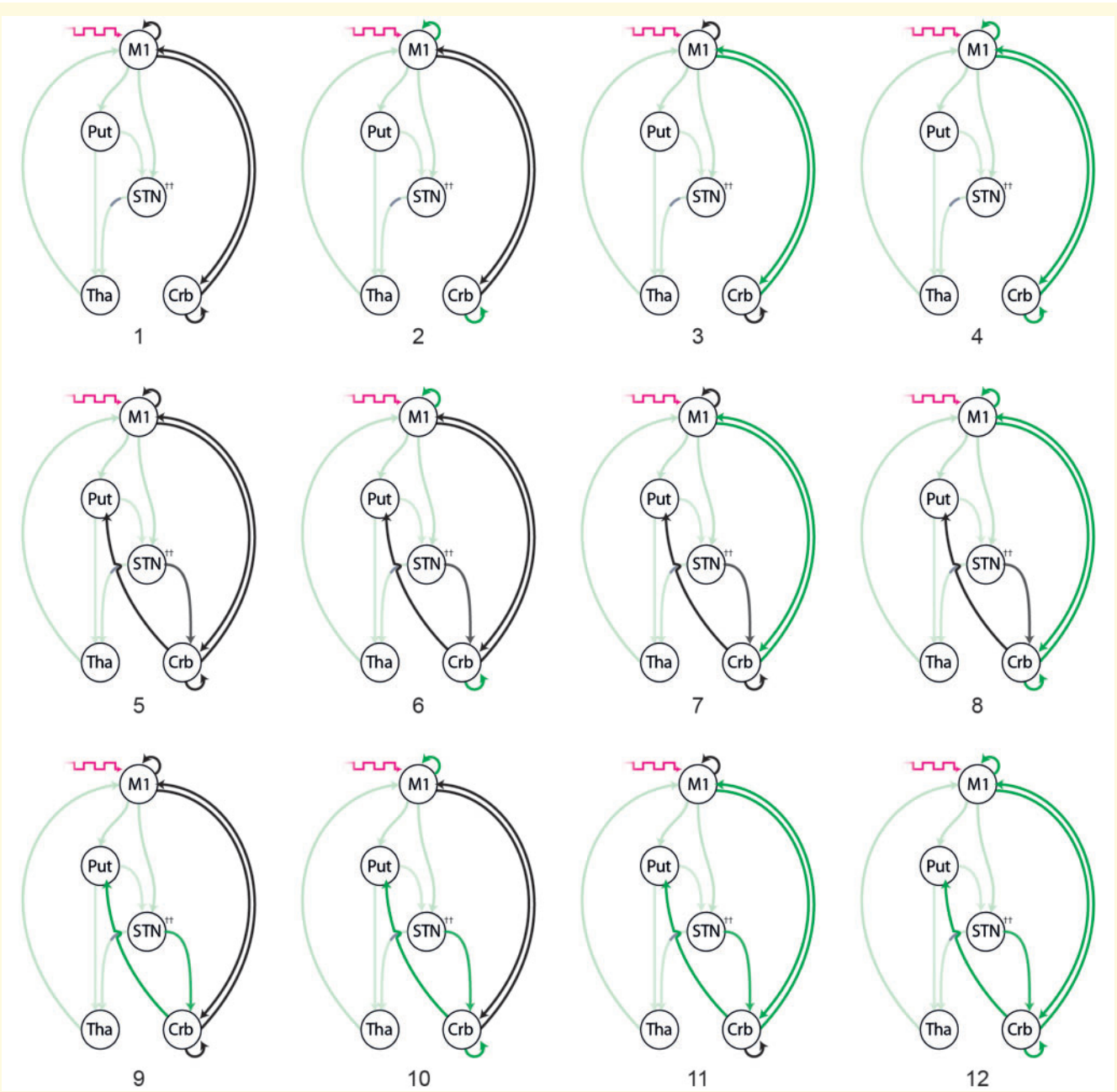


**Figure 1 Experiment II and III model space: 12 competing models of the functional architecture underlying both the voluntary movement and resting states.** For the movement functional MRI data, the main effect of voluntary movement (magenta arrow) drives M1 (DCM C-matrix); this driving input was not present when models were fit to the resting data. Black arrows represent the recruitment of directed effective connectivity during the behavioural state (DCM A-matrix). Green arrows represent modulation of effective connectivity by active DBS during the behavioural state (DCM B-matrix). All models share modulatory effects on basal ganglia pathways, which are highlighted in a lighter green. All models assume that the STN–thalamus (Tha) pathways exerts inhibition on the thalamus. All other pathways are excitatory. Crb = cerebellum; Put = putamen.

Models were subsequently compared across all subjects using BMS (fixed effects assumptions). As previously, the model with the highest model evidence was considered the group winner, from which coupling parameters from each patient were extracted and compared using two-tailed paired *t*-tests.

## Experiment III: The effect of STN DBS on resting state connectivity including cortico-cerebellar circuits

To compare connectivity during the movement task state with the resting state, the resting state data underwent a repeat DCM analysis in an identical way to that described in Experiment II, to incorporate the potential role of cerebellar connectivity. Volume of interest locations from Experiment II were used to guide resting state volume of interest specification, and the same model space was tested, posing the same questions of the data. The only difference was the absence of any explicit driving inputs (DCM C-matrix). Models and coupling parameters were compared in the same way.

## Data availability

The data that support the findings of this study are available from the corresponding author, upon reasonable request.

# Results

## Clinical effect of STN DBS

All patients showed significant clinical improvement. UPDRS-III scores reduced from an average (±standard deviation) of 50 (±15.1) off DBS, to 23.9 (±10.6) on DBS, equivalent to a mean improvement of 52.2% (±12.2%) ($P < 0.05$). Improvements were observed across all sub-domains, and across both hemibodies (Fig. 2).

## Experiment I: Are the effects of STN DBS on resting state connectivity in the basal ganglia motor loop reproducible?

As previously, BMS revealed model 32 to be the most likely generator of the BOLD data at the group level. This model included DBS-related modulatory effects on the cortico-striatal, direct, indirect, hyperdirect and thalamo-cortical pathways. Statistically significant changes in coupling associated with DBS were detected in all connections. The magnitudes of change were much smaller when the coupling involved the STN, as was initially reported in (Kahan *et al.*, 2014). DBS was associated with increased coupling of the cortico-striatal, direct and thalamo-cortical pathways,

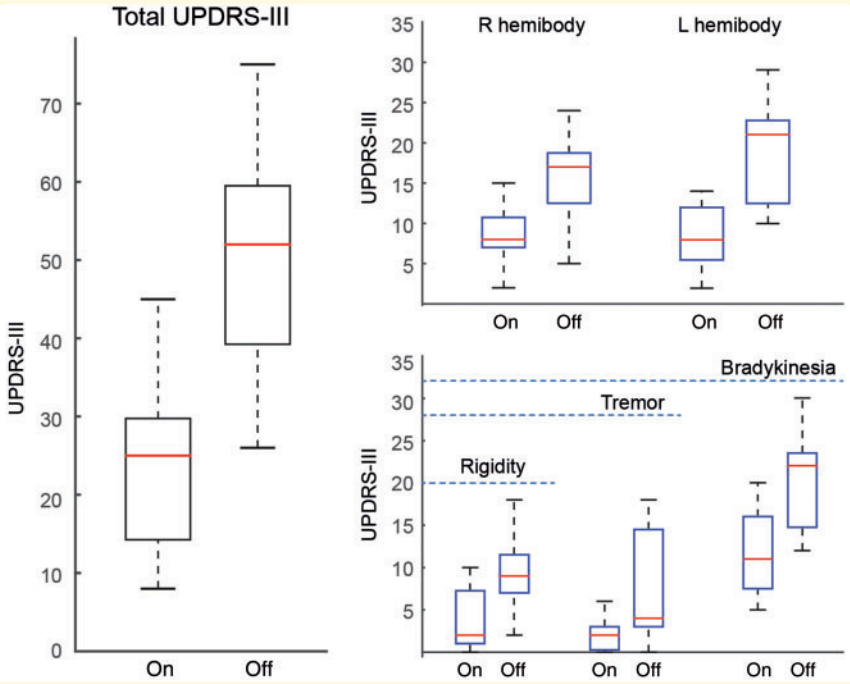


**Figure 2 Clinical improvements following STN DBS.** All scoring was performed off medication. Higher scores confer greater impairment. Total scores were broken down into hemibody scores (not including axial scores), and into subdomains of impairment. Blue dashed line indicates the maximum number of points in the respective subscale. The central mark in each box is the median, the edges of the box are the 25th and 75th percentiles respectively, the whiskers extend to the most extreme data points the algorithm considers to be not outliers. *$P < 0.05$. L = left; R = right.

and reduced coupling of the STN afferents and efferents (Fig. 3).

## Experiment IIa: The effect of STN DBS on peak velocity and reaction time

STN DBS significantly increased $V_{max}$ ($P < 0.05$), but improvements in reaction time were only trend significant ($P = 0.06$) (Fig. 4). To confirm the validity of our analyses, we tested for correlations between $V_{max}$ and total UPDRS-III, and bradykinesia subscores on and off DBS. Only correlations between $V_{max}$ and bradykinesia off scores were statistically significant (on: $r = -0.59$, $P = 0.056$; off: $r = -0.62$, $P = 0.042$) suggesting that $V_{max}$ was better related to bradykinesia than total UPDRS-III scores. No significant effect on directional randomness was detected [mean on Evans random number generator (RNG): 0.54, mean off RNG: 0.56, $P = 0.542$].

## Experiment IIb: The effect of STN DBS on regional voluntary movement-related BOLD responses

Tests for the main effects of movement contrast at the group level revealed characteristic movement task activations, consistent with the PET and functional MRI literature that have used similar tasks. We did not detect any obvious stigmata of motion artefact (e.g. cortical 'rims' or spurious ventricular activations).

The group-level Movement × DBS on > off contrast revealed two large clusters that survived whole brain correction, precisely located in the precentral gyrus hand area, and midline cerebellum (Table 2 and Fig. 4). We did not detect any significant DBS-related reductions in movement-induced regional response using the off > on contrast. The finding of the cerebellar cluster motivated the inclusion of cortico-cerebellar coupling into our previously reported basal ganglia DCM.

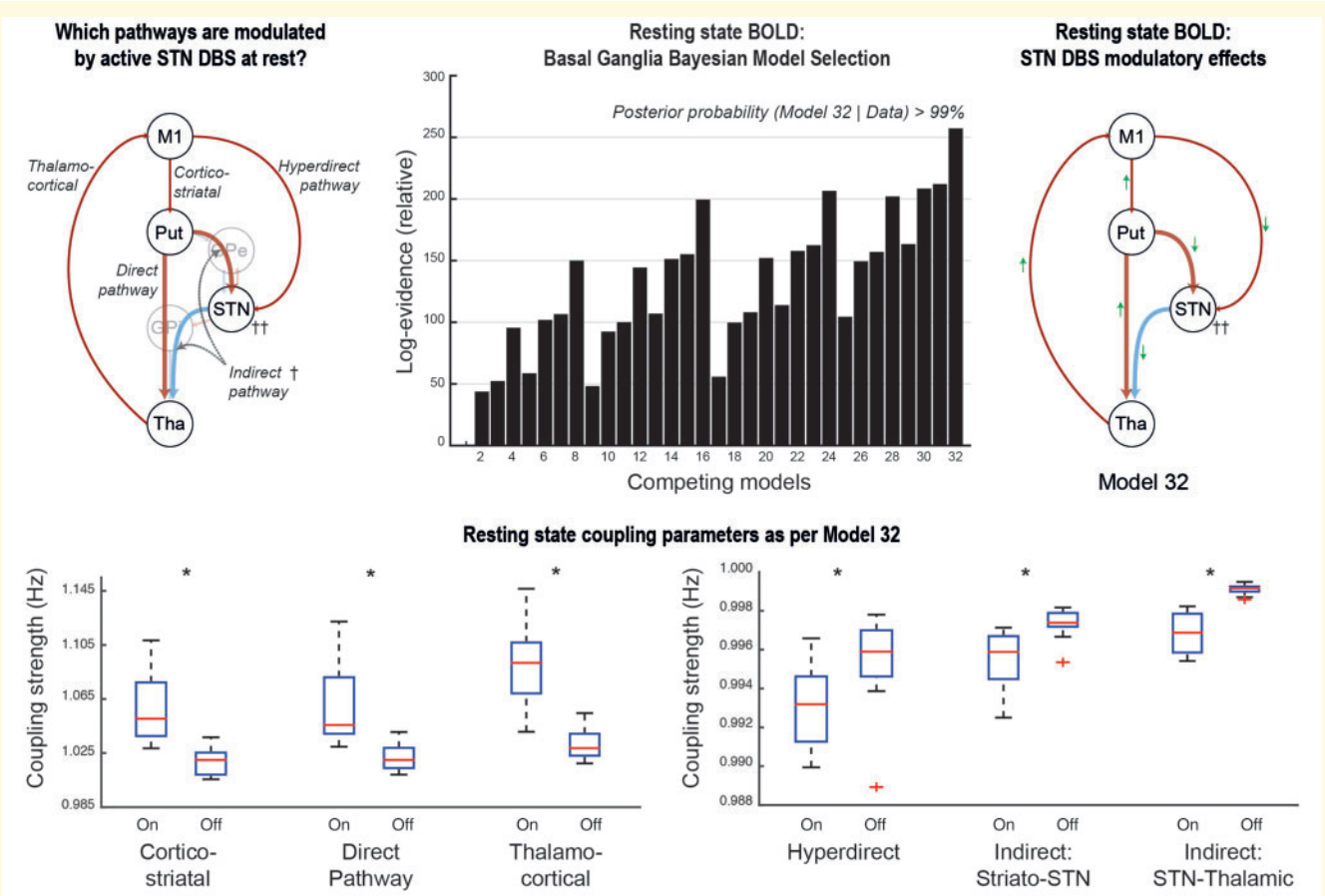


**Figure 3 Experiment I model comparisons and coupling parameters: BMS revealed that model 32 was the most likely generator of the data.** The direction of modulatory effects on the various basal ganglia pathways are summarized by the green arrows. Red arrows represent excitatory effective connectivity, whereas blue arrows represent inhibitory effective connectivity. *T*-tests revealed significant differences in all coupling parameters associated with active DBS. Note the difference in scale for the indirect and hyperdirect pathways compared to the direct pathway. The central mark in each box is the median, the edges of the box are the 25th and 75th percentiles, respectively, the whiskers extend to the most extreme data points the algorithm considers to be not outliers. *$P < 0.05$ corrected for multiple comparisons using the Bonferroni procedure.

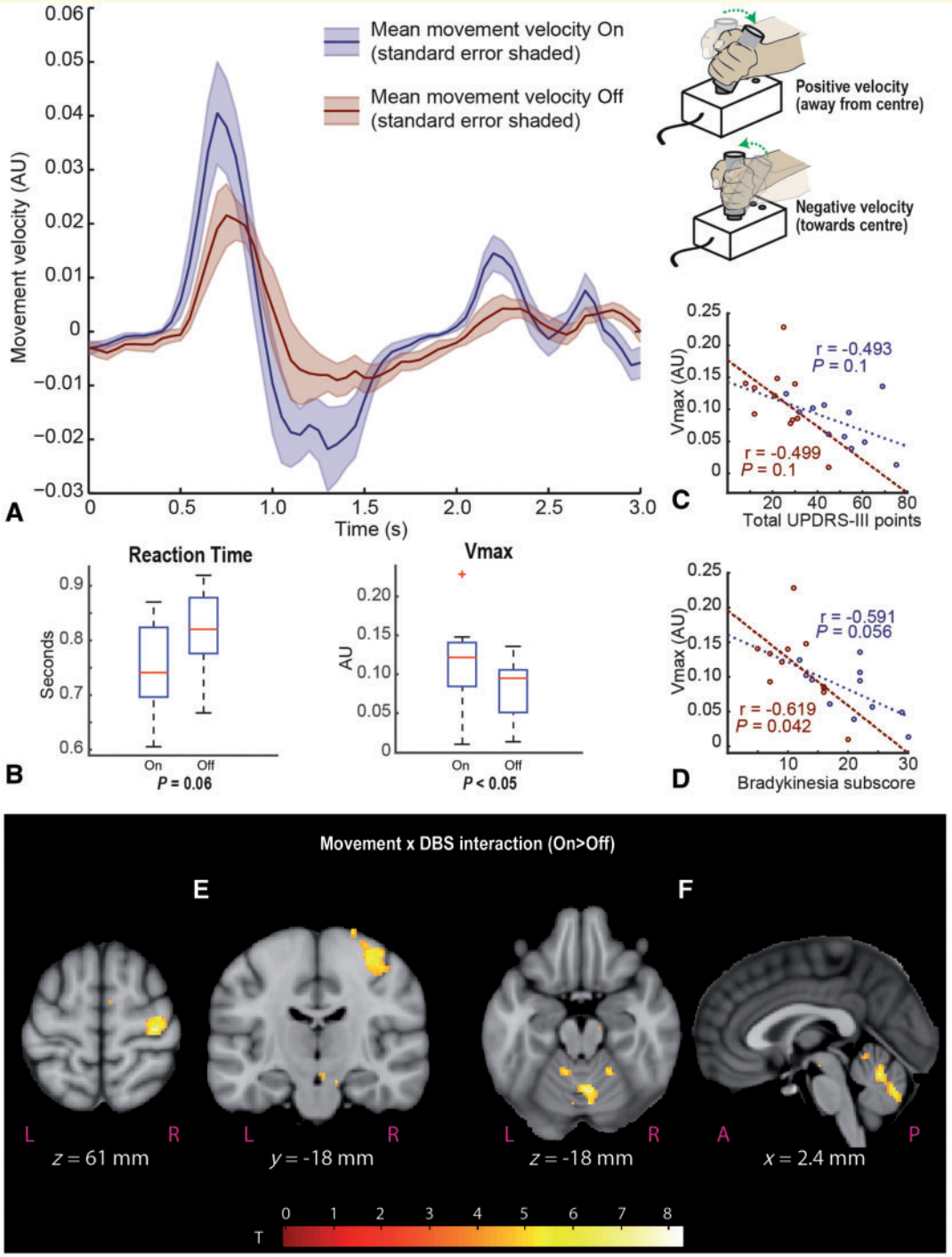


**Figure 4 The effect of DBS on $V_{max}$ and reaction time and regional BOLD activity.** (**A**) The mean velocity plot for a single movement trial – on and off compared. Cue sounds at time = 0 with joystick in central position. Positive velocity occurs when subject moves joystick away from the central position towards their chosen direction, slows to 0 at maximal displacement, then velocity is negative as the handle is returned to the centre position. (**B**) Mean reaction time and $V_{max}$ on and off stimulation. Note that reaction time differences are only trend significant. (**C** and **D**) Scatter plots of total UPDRS score, and bradykinesia sub-score against $V_{max}$. Maroon plots represent off values, blue plots represent on values. Two clusters were identified as significant following whole brain correction in (**E**) M1 hand area contralateral to movements, and (**F**) midline cerebellum encompassing left crus V, vermis and right crus V and VI. Second level SPMs overlaid on the MNI brain. SPMs are thresholded at a voxel level of $P < 0.001$ (uncorrected), cluster extent threshold = 0. Additional activations at this threshold can be seen in the supplementary motor area and midbrain (**E**), although these did not survive cluster-wise corrected significance.

**Table 2 Results of a group (i.e. second level) whole brain search for Movement × DBS on > off interaction**

| Cluster-wise | | | Peak-wise | | | MNI coordinates, mm | | |
|---|---|---|---|---|---|---|---|---|
| $P_{FWE}$ | Voxels | $P_{unc}$ | T | Z | $P_{unc}$ | x | y | z |
| 0.00180 | 245 | $9.4 \times 10^{-5}$ | 8.27 | 4.44 | $4.4 \times 10^{-6}$ | 6 | −60 | −18 |
| Cluster B in Fig. 4 | | | 6.46 | 3.97 | $3.6 \times 10^{-5}$ | 4 | −70 | −30 |
| | | | 6.36 | 3.94 | $4.1 \times 10^{-5}$ | −2 | −60 | −22 |
| 0.00010 | 369 | $5.1 \times 10^{-6}$ | 7.79 | 4.33 | $7.4 \times 10^{-6}$ | 34 | −22 | 60 |
| Cluster A in Fig. 4 | | | 6.06 | 3.84 | $6.1 \times 10^{-5}$ | 42 | −14 | 52 |
| | | | 5.73 | 3.73 | $9.5 \times 10^{-5}$ | 30 | −22 | 70 |

Clusters surviving cluster-wise significance (corrected using the family wise error correction for multiple comparisons = $P_{FWE}$) of $P < 0.05$ were considered significant. Two clusters were found to be significant, one 245 voxel cluster in the cerebellum, and one 369 voxel cluster in the precentral gyrus. The three peak voxels of each cluster are reported. $P_{unc}$ = uncorrected *P*-values. A cerebellar atlas normalized to MNI space using FLIRT (Diedrichsen *et al.*, 2009) revealed that the cerebellar cluster encompassed the left crus V, as well as the vermis and right-sided crus V and VI.

## Experiment IIc: The effect of STN DBS on cortico-basal ganglia and cerebellar dynamics during voluntary movements

BMS revealed model 10 to be the most likely generator of the BOLD data at the group level (posterior probability >99%). This model included the cerebellum reciprocally connected to both M1 and the basal ganglia, suggesting that voluntary movements engage both pathways. DBS-related modulatory effects impacted on the cortico-striatal, direct, indirect, hyperdirect and thalamo-cortical pathways, as well as both M1 and cerebellar intrinsic coupling, and the reciprocal subcortical connections, but not the cortico-cerebellar projections. DBS was associated with statistically significant changes (corrected using the Bonferroni procedure) in coupling at the group level for the M1 and cerebellar intrinsic coupling, the cerebellar projection to the putamen, the STN afferent projections, and the STN efferent to the thalamus. DBS decreased the self-inhibitory tone of both M1 and cerebellum, and increased coupling in all other connections except for STN projections to the thalamus (Fig. 5).

## Experiment III: The effect of STN DBS on cortico-basal ganglia and cerebellar dynamics during rest

In contrast to the movement task state, BMS revealed model 1 to be the most likely generator of the resting state BOLD data at the group level (posterior probability >99%). This model had the cerebellum reciprocally connected to M1, with no significant cerebellar-subcortical resting state coupling. DBS-related modulatory effects impacted on the cortico-striatal, direct, indirect, hyperdirect and thalamo-cortical pathways, with no effects on any of the cerebellar pathways or local circuitry. Statistically-significant changes in coupling associated with DBS were detected in the STN afferent and efferent connections at the group level (corrected using the Bonferroni procedure). The directions of change in the basal ganglia circuit were notably different to those found when the data were analysed during the movement task, likely related to the different generative model (Fig. 5).

As an exploratory analysis, we then looked for correlations between coupling strengths of connections modulated by DBS during the movement task, and the $V_{max}$. We then repeated this for coupling strengths calculated during the resting state. Correlations were found between $V_{max}$ and coupling in the M1 and cerebellar self-inhibition, the STN afferent projections, and the STN projection to the cerebellum. Of note, with regards the STN afferent connections, stronger coupling during movement were associated with a greater $V_{max}$. However, when the same correlations were explored during rest, stronger coupling at rest were associated with a slower $V_{max}$ (during movement) (Fig. 6). The caveat to this analysis is that because the data were generated by different models, it is difficult to compare their respective parameters.

# Discussion

In this series of experiments, we use rare *in vivo* human data from patients with Parkinson's disease and chronically implanted therapeutic STN DBS, to expand on our previous modelling of the basal ganglia, allowing us to dissect the effects of DBS on functional integration within the motor system.

## STN DBS is associated with reproducible changes in basal ganglia coupling at rest

Data from this independent patient cohort treated in the same centre reveal that STN DBS is associated with strengthening of the direct (cortico-striatal and thalamo-cortical) coupling, and a reduction in hyperdirect (striato-STN and STN-thalamic) coupling while patients lie at rest. This appears to remain largely true, even when cerebellar dynamics are also modelled, although the changes in

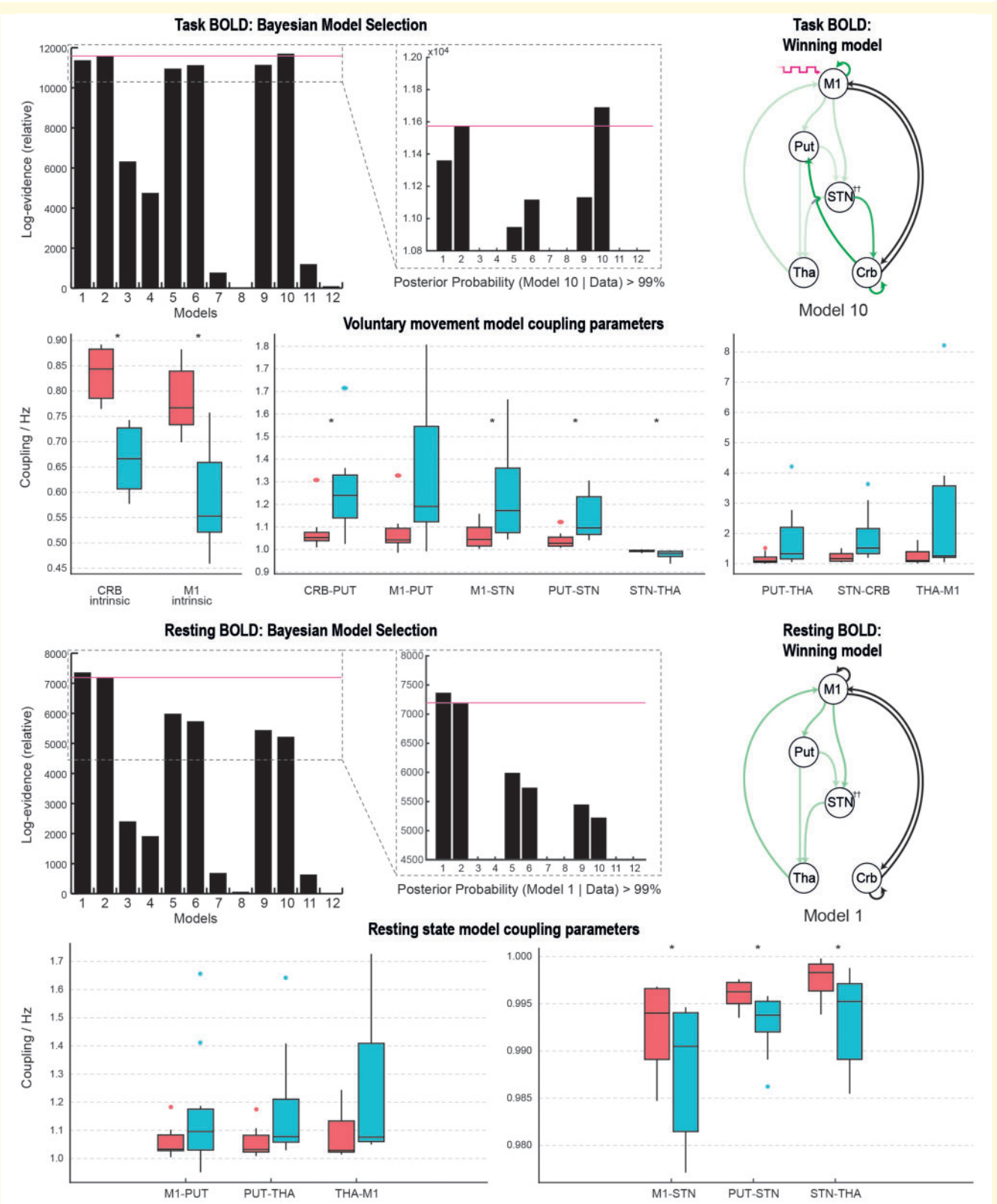


**Figure 5 Model comparisons and coupling parameters: model comparison revealed that model 10 was the most likely generator of the movement data.** Green arrows represent the pathways modulated by DBS. Black arrows represent non-modulated pathways engaged during voluntary movement. Box plots represent the distribution (median, interquartile range) of coupling strength values on (blue) and off (red) DBS across 11 subjects. Paired *t*-tests of these values revealed statistically significant changes in coupling strengths in 7 of 10 pathways founds to be modulated by DBS. Coloured circles represent data points considered to be outliers. Model comparison revealed that model 1 was the most likely generator of the resting state data. Green arrows represent the pathways modulated by DBS. Black arrows represent non-modulated pathways engaged during rest. $^{*}P < 0.05$ (Bonferroni corrected). Crb/CRB = cerebellum; Put/PUT = putamen; Tha/THA = thalamus.

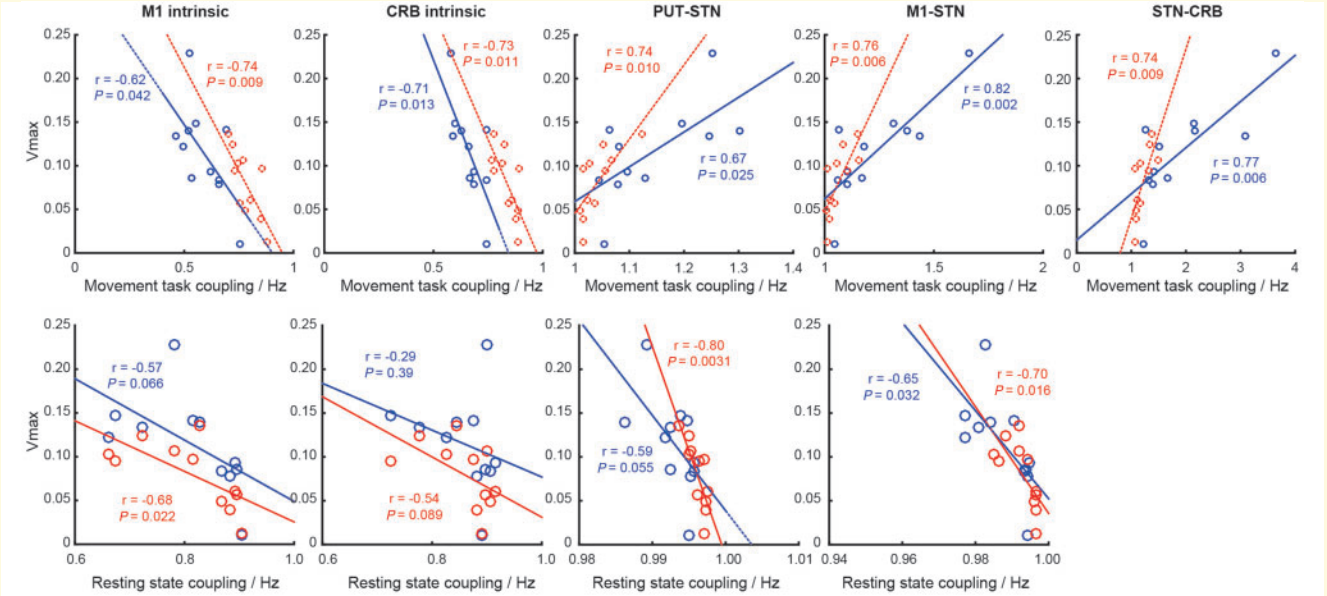


**Figure 6 Exploratory correlation analysis looking for relationships between coupling strength and measured peak movement velocity ($V_{max}$).** Blue data points and lines of best fit represent DBS on, red data points and lines of best fit represent DBS off. Pearson's r and *P*-values are reported in line. CRB = cerebellum; Put = putamen.

cortico-striatal, direct and thalamo-cortical pathways did not survive our conservative statistical thresholding for multiple comparisons. The reduction of both afferent and efferent effective connectivity of the STN appears consistent with neural field models of the basal ganglia and effects of DBS, which demonstrate DBS-related mean membrane potential perturbations and reduction in network loop gains (Müller and Robinson, 2018). Our previous study (Kahan *et al.*, 2014) recruited a cohort who were slightly older (mean age 57 versus 53), and who had been undergoing chronic therapeutic stimulation for longer (mean time since surgery 38 months versus 18 months). Data collection also differed; this cohort was scanned using the body-transmit coil and 12-channel head receive-only coil (Kahan *et al.*, 2015), whereas previous data used a transmit-receive head coil. Analysis of this cohort was limited to the right hemisphere because only right hemisphere functional localization data were available, which effectively constrained our *n* to 11 hemispheres. Despite these differences, the modelled effective connectivity parameters, and the modulatory effects related to DBS were consistent.

## Therapeutic STN DBS improves motor performance and increases motor-evoked responses in M1 and cerebellum

This study found STN DBS significantly increased BOLD activity during voluntary movements in both M1 and the cerebellum, as has been previously demonstrated using $H_2{}^{15}O$ PET in unilateral DBS patients (Payoux *et al.*, 2004). STN DBS has been shown to produce both increased and decreased evoked responses in different parts of the lateral cerebellar cortex during movements (Grafton *et al.*, 2006), and changes in resting cerebellar metabolism have been widely reported, in both the vermis (Sestini *et al.*, 2002; Asanuma *et al.*, 2006; Cilia *et al.*, 2009; Bradberry *et al.*, 2012), and lateral cerebellar cortex (Hershey *et al.*, 2003; Vafaee *et al.*, 2004; Nagaoka *et al.*, 2007; Tanei *et al.*, 2009; Wang *et al.*, 2010; Garraux *et al.*, 2011; Volonté *et al.*, 2012). The cluster detected in this cohort is relatively medial; however, probabilistic cerebellar atlases (Diedrichsen *et al.*, 2009) suggest that the peak cluster is centred on the right cerebellar V (probability 83%). As is evident from Fig. 2, a number of the patients saw significant improvements in tremor with active STN DBS. Tremor has previously been associated with increased activity in both M1 and cerebellum (Helmich *et al.*, 2011; Mure *et al.*, 2011), and improvement during active DBS may have led to an underestimation of movement-related activity in both these regions, which might have contributed to the significant Movement × DBS interaction demonstrated.

## State-dependent integration of basal ganglia and cerebellar dynamics

Comparing the BMS results of data collected during a movement task, and data collected at rest revealed a number of interesting and novel insights. First, during the resting state, cerebellar integration appears to engage cortico-cerebellar projections predominantly; models including subcortical pathways were less likely to generate the data at rest. This is not to say that the anatomical pathways do not exist, rather that they are not engaged. It is important to

note that the anatomical substrate of our modelled cerebellar-cortical pathways are likely polysynaptic projections via the ventral-intermediate/ventral-lateral posterior (Vim/VLp) thalamus (which is absent from our model). Our thalamic node, which summarizes the output of the basal ganglia, would more accurately represent the ventral-lateral anterior (VLa), ventral-anterior parvicellular (VApc) and ventral-medial (VM) nuclei.

In contrast, when the patient switches their behavioural state to perform a movement task, the reciprocal connections between the basal ganglia and cerebellum are additionally recruited. Anatomical evidence from primates suggests that cerebellar fibres project polysynaptically, arriving at the striatum, and connectivity from the basal ganglia to cerebellum is mediated through the STN (Hoshi *et al.*, 2005; Bostan *et al.*, 2010), and thus those specific pathways were included in our model space.

## State-dependent modulatory effects of STN DBS

We also demonstrate that the modulatory effects of STN DBS appear to be similarly dependent on the behavioural state. The recruitment of the subcortical pathways during movement significantly changes the resulting coupling strength estimates—most strikingly when looking at the effect of DBS on STN afferent coupling. During rest, DBS reduced coupling along the hyperdirect pathway and indirect pathways. This was first identified in our previous work (Kahan *et al.*, 2014), where it was noted that although STN DBS reduced hyperdirect coupling, patients with stronger hyperdirect coupling had fewer symptoms. Our exploratory correlation analysis (Fig. 6), contradicts this finding at rest, showing that stronger hyperdirect coupling during rest is associated with a slower peak velocity in our objective movement task. During movement, however, STN DBS increases both hyperdirect and striatal-STN afferents, and correlation analysis reveals stronger coupling of both of those pathways is associated with faster peak velocities. In addition, models including modulatory effects on intrinsic coupling (i.e. local self-inhibitory tone) were more favourable than without, and intrinsic coupling in both the cortex and cerebellum was correlated (albeit weakly) with movement speed. Dirkx *et al.* (2016, 2017) have seen similar results when exploring the impact of levodopa on resting tremor and intrinsic Vim coupling. Of additional interest would be to identify how these connectivity changes relate to changes in beta (13–30 Hz) phase and cortical broadband gamma activity (50–200 Hz), also implicated as relevant to the mechanism of action of STN DBS (de Hemptinne *et al.*, 2013, 2015). Modelling of electrophysiological data has also implicated cortical inhibitory subpopulations in the generation of cortical beta activity (Reis *et al.*, 2019).

Given the models differed between movement and resting states, it is difficult to compare their respective coupling parameters. The fundamental finding is that the most likely model generating the movement data is different to that generating the rest data, both in terms of connections recruited by the behaviour, and connections impacted by DBS.

## Limitations

A prominent source of noise in functional MRI is motion of the subject during scanning, producing both spin-history and susceptibility-by-movement artefacts (Friston *et al.*, 1996; Wu *et al.*, 1997; Andersson *et al.*, 2001). As a means of nullifying this, specialist padding was used to fixate the patients' heads in the MRI head coil. Furthermore, data were first realigned and unwarped. Despite our efforts, we observed a degree of collinearity between head position and the main effect of movement condition. As a result, head position confounds were explicitly excluded from first level GLMs in Experiments II and III to maximize the efficiency with which voluntary movement responses were estimated. This efficiency would have been compromised by the inclusion of correlated or collinear head motion confounds (Farrar and Glauber, 1967; Friston *et al.*, 1994). This said, the DCM analyses are in principle less susceptible to instantaneous signal fluctuations related to motion, because DCM can only model the delayed haemodynamic response (Friston *et al.*, 2003). Nevertheless it is important that the results of Experiment II are interpreted in the context of a potential head motion confound (this applies only to the main effects of movement, not the interaction with stimulation, or the corresponding modulatory effects of DBS on connectivity).

Our models make a number of simplifying assumptions, most notably the absence of pallidal dynamics, and the sparsity of connections amongst the nodes. DCM does not necessarily quantify monosynaptic coupling, thus not all intermediate nodes are required to estimate effective connectivity between any two nodes. We have modelled DBS as a modulatory effect on coupling, not as a driving input to individual nodes. Thus, changes in coupling parameters do not inform us of how DBS reaches modulated nodes, or why it modulates them, rather they represent the consequence of the active DBS.

Additionally, due to signal drop-out around the electrode, it was not possible to record BOLD data from the STN itself. Therefore, we modelled the STN as a hidden node, enabling inference on its afferents and efferents based on the influence they exert on nodes from which precise recordings were available (David *et al.*, 2011; Marreiros *et al.*, 2012; Kahan *et al.*, 2014). In principle, our hidden node could be any brain region with the connectivity fingerprint specified by the model (i.e. any brain region excited by both M1 and the putamen, and that exerts inhibition on the thalamus). Given the anatomical and electrophysiological literature on the functional anatomy of the basal ganglia, our hidden node was attributed to the STN.

We assumed that within our patient cohort, STN DBS consistently modulates the same subset of connections. In other words, the model underlying each patient's data is the same (i.e. fixed). The degree of modulation of each connection, however, varies from patient to patient randomly. This is in contrast to assuming that different patients have different connections modulated by DBS, as well as varying degrees of modulation. As such, a fixed effects BMS analysis was chosen as the most appropriate means of identifying the most likely single generative model given the observed data. By performing a random effects BMS analysis, we would be implicitly supporting what we feel to be an untenable assumption (Friston *et al.*, 1999, 2015; Stephan *et al.*, 2009; Rigoux *et al.*, 2013; Litvak *et al.*, 2015). In line with this, we used paired *t*-tests to explore the effect of DBS in relation to random effects on the parameters over subjects.

Medication was withdrawn for 10–12 h before scanning, with a view to looking specifically at the effects of DBS, and maximizing the clinical contrast between the experimental conditions. In other words, had we performed the study in the context of medications, not only would the results be confounded by the pharmacodynamics of the medications, but also the clinical impact of DBS would be more subtle, perhaps making the neurobiological substrate more difficult to detect. The length of medication withdrawal was not empirically determined based on medication pharmacodynamics, but was pragmatic, so we cannot rule out some medication confounding effects. The impact of dopaminergic medications on the basal ganglia network has been looked at in similar studies (Dirkx *et al.*, 2017), but the specific effects on our proposed model require further study, especially given the substantial variability in medication doses in our small cohort.

We were able to recruit a typical cohort of Parkinson's disease patients with STN DBS, however it should be noted that the patients were all able to travel a short distance to the hospital in the morning having not had their morning medications, lie relatively still, and tolerate being in the scanner for 1–2 h. Thus our findings might not generalize to those unable to meet such criteria.

# Conclusions

We demonstrate that active STN DBS is associated with reproducible changes in effective connectivity within the cortico-basal ganglia motor loop. We then show that during voluntary movement task functional MRI, active STN DBS was associated with increased activity in the primary motor cortex and midline cerebellar cortex. Modelling of these data reveals that (i) patients with Parkinson's disease demonstrate behaviour dependent recruitment of basal ganglia–cerebellar connections that are preferentially engaged during movement and not rest; and (ii) STN DBS has behaviour dependent modulatory effects on pathways within the motor system, as well as behaviour-independent changes.

# Acknowledgements

The authors acknowledge the use of the UCL Legion High Performance Computing Facility (Legion@UCL), and associated support services, in the completion of this work.

# Funding

This study was funded by the Brain Research trust (www.brt.org.uk). J.K. received funding from The Astor Foundation, The Rosetrees Trust, and the MHMS General Charitable Trust. T.F., L.Z., M.H. and the Unit of Functional Neurosurgery are funded by the Parkinson's Appeal and the Monument trust. T.F. also receives funding from Cure Parkinson's Trust, Parkinson's UK, John Black Charitable Foundation and the Michael J Fox Foundation. K.J.F. is funded by a Wellcome Trust Principal Research Fellowship (Ref: 088130/Z/09/Z). The work was undertaken by UCL/UCLH, who receives a proportion of funding from the UK Department of Health's NIHR Biomedical Research Centres funding scheme. The funders had no role in study design, data collection and analysis, decision to publish, or preparation of the manuscript. We confirm that any author affiliations or competing interests had no impact on the data.

# Competing interests

T.F., L.Z., M.H., and P.L. report that they have received honoraria from industry for invited talks. J.K. has received funding from Medtronic for academic conference travel. There are no patents, products in development or marketed products to declare.

# Supplementary material

Supplementary material is available at *Brain* online.

# References

Albin RL, Young AB, Penney JB. The functional anatomy of basal ganglia disorders. Trends Neurosci. 1989; 12: 366–75.

Andersson JL, Hutton C, Ashburner J, Turner R, Friston K. Modeling geometric deformations in EPI time series. Neuroimage 2001; 13: 903–19.

Asanuma K, Tang C, Ma Y, Dhawan V, Mattis P, Edwards C, et al. Network modulation in the treatment of Parkinson's disease. Brain 2006; 129: 2667–78.

Behrens TEJ, Johansen-Berg H, Woolrich MW, Smith SM, Wheeler-Kingshott CAM, Boulby PA, et al. Non-invasive mapping of connections between human thalamus and cortex using diffusion imaging. Nat Neurosci 2003; 6: 750–57.

Beurrier C, Bioulac B, Audin J, Hammond C. High-frequency stimulation produces a transient blockade of voltage-gated currents in subthalamic neurons. J Neurophysiol 2001; 85: 1351–6.

Boertien T, Zrinzo L, Kahan J, Jahanshahi M, Hariz M, Mancini L, et al. Functional imaging of subthalamic nucleus deep brain stimulation in Parkinson's disease. Mov Disord 2011; 26: 1835–43.

Bostan AC, Dum RP, Strick PL. The basal ganglia communicate with the cerebellum. Proc Natl Acad Sci U S A 2010; 107: 8452–56.

Bradberry TJ, Metman LV, Contreras-Vidal JL, van den Munckhof P, Hosey LA, Thompson JLW, et al. Common and unique responses to dopamine agonist therapy and deep brain stimulation in Parkinson's disease: an H(2)(15)O PET study. Brain Stimul 2012; 5: 605–15.

Ceballos-Baumann AO, Boecker H, Bartenstein P, von Falkenhayn I, Riescher H, Conrad B, et al. A positron emission tomographic study of subthalamic nucleus stimulation in Parkinson disease: enhanced movement-related activity of motor-association cortex and decreased motor cortex resting activity. Arch Neurol 1999; 56: 997–1003.

Cilia R, Marotta G, Landi A, Isaias IU, Mariani CB, Vergani F, et al. Clinical and cerebral activity changes induced by subthalamic nucleus stimulation in advanced Parkinson's disease: a prospective case-control study. Clin Neurol Neurosurg 2009; 111: 140–6.

David O, Maess B, Eckstein K, Friederici AD. Dynamic causal modeling of subcortical connectivity of language. J Neurosci 2011; 31: 2712–7.

DeLong MR. Primate models of movement disorders of basal ganglia origin. Trends Neurosci 1990; 13: 281–5.

Deniau J-M, Degos B, Bosch C, Maurice N. Deep brain stimulation mechanisms: beyond the concept of local functional inhibition. Eur J Neurosci 2010; 32: 1080–91.

Deuschl G, Schade-Brittinger C, Krack P, Volkmann J, Schäfer H, Bötzel K, et al. A randomized trial of deep-brain stimulation for Parkinson's disease. N Engl J Med 2006; 355: 896–908.

Diedrichsen J, Balsters JH, Flavell J, Cussans E, Ramnani N. A probabilistic MR atlas of the human cerebellum. Neuroimage 2009; 46: 39–46.

Dirkx MF, den Ouden H, Aarts E, Timmer M, Bloem BR, Toni I, et al. The cerebral network of Parkinson's tremor: an effective connectivity fMRI study. J Neurosci 2016; 36: 5362–72.

Dirkx MF, den Ouden HEM, Aarts E, Timmer MHM, Bloem BR, Toni I, et al. Dopamine controls Parkinson's tremor by inhibiting the cerebellar thalamus. Brain 2017; 140: 721–34.

Eusebio A, Thevathasan W, Doyle Gaynor L, Pogosyan A, Bye E, Foltynie T, et al. Deep brain stimulation can suppress pathological synchronisation in parkinsonian patients. J Neurol Neurosurg Psychiatry 2011; 82: 569–73.

Farrar DE, Glauber RR. Multicollinearity in regression analysis: the problem revisited. Rev Econ Stat 1967; 49: 92–107.

Foltynie T, Zrinzo L, Martinez-Torres I, Tripoliti E, Petersen E, Holl E, et al. MRI-guided STN DBS in Parkinson's disease without microelectrode recording: efficacy and safety. J Neurol Neurosurg Psychiatry 2011; 82: 358–63.

Friston K, Stephan K, Li B, Daunizeau J. Generalised filtering. Math Probl Eng 2010; 2010: 1–34.

Friston K, Zeidman P, Litvak V. Empirical Bayes for DCM: a group inversion scheme. Front Syst Neurosci 2015; 9: 164.

Friston KJ, Buechel C, Fink GR, Morris J, Rolls E, Dolan RJ. Psychophysiological and modulatory interactions in neuroimaging. Neuroimage 1997; 6: 218–29.

Friston KJ, Harrison L, Penny W. Dynamic causal modelling. Neuroimage 2003; 19: 1273–302.

Friston KJ, Holmes AP, Price CJ, Büchel C, Worsley KJ. Multisubject fMRI studies and conjunction analyses. Neuroimage 1999; 10: 385–96.

Friston KJ, Jezzard P, Turner R. Analysis of functional MRI time-series. Hum Brain Mapp 1994; 1: 153–71.

Friston KJ, Williams S, Howard R, Frackowiak RS, Turner R. Movement-related effects in fMRI time-series. Magn Reson Med 1996; 35: 346–55.

Garraux G, Bahri MA, Lemaire C, Degueldre C, Salmon E, Kaschten B. Brain energization in response to deep brain stimulation of subthalamic nuclei in Parkinson's disease. J Cereb Blood Flow Metab 2011; 31: 1612–22.

Grafton ST, Turner RS, Desmurget M, Bakay R, Delong M, Vitek J, et al. Normalizing motor-related brain activity: subthalamic nucleus stimulation in Parkinson disease. Neurology 2006; 66: 1192–9.

Gratwicke J, Kahan J, Zrinzo L, Hariz M, Limousin P, Foltynie T, et al. The nucleus basalis of Meynert: a new target for deep brain stimulation in dementia? Neurosci Biobehav Rev 2013; 37: 2676–88.

Helmich RC, Janssen MJR, Oyen WJG, Bloem BR, Toni I. Pallidal dysfunction drives a cerebellothalamic circuit into Parkinson tremor. Ann Neurol 2011; 69: 269–81.

de Hemptinne C, Ryapolova-Webb ES, Air EL, Garcia PA, Miller KJ, Ojemann JG, et al. Exaggerated phase-amplitude coupling in the primary motor cortex in Parkinson disease. Proc Natl Acad Sci U S A 2013; 110: 4780–5.

de Hemptinne C, Swann NC, Ostrem JL, Ryapolova-Webb ES, San Luciano M, Galifianakis NB, et al. Therapeutic deep brain stimulation reduces cortical phase-amplitude coupling in Parkinson's disease. Nat Neurosci. 2015; 18: 779–86.

Hershey T, Revilla FJ, Wernle AR, McGee-Minnich L, Antenor JV, Videen TO, et al. Cortical and subcortical blood flow effects of subthalamic nucleus stimulation in PD. Neurology 2003; 61: 816–21.

Holiga Š, Mueller K, Möller HE, Urgošík D, Růžička E, Schroeter ML, et al. Resting-state functional magnetic resonance imaging of the subthalamic microlesion and stimulation effects in Parkinson's disease: indications of a principal role of the brainstem. NeuroImage Clin 2015; 9: 264–74.

Holtzheimer PE, Mayberg HS. Deep brain stimulation for psychiatric disorders. Annu Rev Neurosci 2011; 34: 289–307.

Hoshi E, Tremblay L, Féger J, Carras PL, Strick PL. The cerebellum communicates with the basal ganglia. Nat Neurosci 2005; 8: 1491–493.

Jech R, Mueller K, Urgošík D, Sieger T, Holiga Š, Růžička F, et al. The subthalamic microlesion story in Parkinson's disease: electrode insertion-related motor improvement with relative cortico-subcortical hypoactivation in fMRI. PLoS One 2012; 7: e49056.

Jech R, Urgosík D, Tintera J, Nebuzelský A, Krásenský J, Liscák R, et al. Functional magnetic resonance imaging during deep brain stimulation: a pilot study in four patients with Parkinson's disease. Mov Disord 2001; 16: 1126–32.

Kahan J, Foltynie T. Understanding DCM: ten simple rules for the clinician. Neuroimage 2013; 83: 542–9.

Kahan J, Mancini L, Urner M, Friston K, Hariz M, Holl E, et al. Therapeutic subthalamic nucleus deep brain stimulation reverses cortico-thalamic coupling during voluntary movements in Parkinson's disease. PLoS One 2012; 7: e50270.

Kahan J, Papadaki A, White M, Mancini L, Yousry T, Zrinzo L, et al. The safety of using body-transmit MRI in patients with implanted deep brain stimulation devices. PLoS One 2015; 10: e0129077.

Kahan J, Urner M, Moran R, Flandin G, Marreiros A, Mancini L, et al. Resting state functional MRI in Parkinson's disease: the impact of deep brain stimulation on 'effective' connectivity. Brain 2014; 137: 1130–44.

Ko JH, Mure H, Tang CC, Ma Y, Dhawan V, Spetsieris P, et al. Parkinson's disease: increased motor network activity in the absence of movement. J Neurosci 2013; 33: 4540–9.

Kühn AA, Kempf F, Brücke C, Gaynor Doyle L, Martinez-Torres I, Pogosyan A, et al. High-frequency stimulation of the subthalamic nucleus suppresses oscillatory beta activity in patients with Parkinson's disease in parallel with improvement in motor performance. J Neurosci 2008; 28: 6165–73.

Laxton AW, Tang-Wai DF, McAndrews MP, Zumsteg D, Wennberg R, Keren R, et al. A phase I trial of deep brain stimulation of memory circuits in Alzheimer's disease. Ann Neurol 2010; 68: 521–34.

Li B, Daunizeau J, Stephan KE, Penny W, Hu D, Friston K. Generalised filtering and stochastic DCM for. Neuroimage 2011; 58: 442–57.

Li Q, Ke Y, Chan DCW, Qian Z-M, Yung KKL, Ko H, et al. Therapeutic deep brain stimulation in Parkinsonian rats directly influences motor cortex. Neuron 2012; 76: 1030–41.

Limousin P, Greene J, Pollak P, Rothwell J, Benabid AL, Frackowiak R. Changes in cerebral activity pattern due to subthalamic nucleus or internal pallidum stimulation in Parkinson's disease. Ann Neurol 1997; 42: 283–91.

Limousin P, Krack P, Pollak P, Benazzouz A, Ardouin C, Hoffmann D, et al. Electrical stimulation of the subthalamic nucleus in advanced Parkinson's disease. N Engl J Med 1998; 339: 1105–11.

Limousin P, Pollak P, Benazzouz A, Hoffmann D, Le Bas JF, Broussolle E, et al. Effect of Parkinsonian signs and symptoms of bilateral subthalamic nucleus stimulation. Lancet 1995; 345: 91–5.

Litvak V, Garrido M, Zeidman P, Friston K. Empirical Bayes for Group (DCM) studies: a reproducibility study. Front Hum Neurosci 2015; 9: 670.

Marreiros AC, Kiebel SJ, Friston KJ. Dynamic causal modelling for fMRI: a two-state model. Neuroimage 2008; 39: 269–78.

Marreiros AC, Cagnan H, Moran RJ, Friston KJ, Brown P. Basal ganglia-cortical interactions in Parkinsonian patients. Neuroimage 2012; 66C: 301.

Maurice N, Thierry A-M, Glowinski J, Deniau J-M. Spontaneous and evoked activity of substantia nigra pars reticulata neurons during high-frequency stimulation of the subthalamic nucleus. J Neurosci 2003; 23: 9929–36.

McIntyre CC, Hahn PJ. Network perspectives on the mechanisms of deep brain stimulation. Neurobiol Dis 2010; 38: 329–37.

Meissner W, Leblois A, Hansel D, Bioulac B, Gross CE, Benazzouz A, et al. Subthalamic high frequency stimulation resets subthalamic firing and reduces abnormal oscillations. Brain 2005; 128: 2372–82.

Mueller K, Jech R, Růžička F, Holiga Š, Ballarini T, Bezdicek O, et al. Brain connectivity changes when comparing effects of subthalamic deep brain stimulation with levodopa treatment in Parkinson's disease. NeuroImage Clin 2018; 4: 1–21.

Mueller K, Jech R, Schroeter ML. Deep-brain stimulation for Parkinson's disease. N Engl J Med 2013; 368: 482–3.

Müller EJ, Robinson PA. Quantitative theory of deep brain stimulation of the subthalamic nucleus for the suppression of pathological rhythms in Parkinson's disease. PLOS Comput Biol 2018; 14: e1006217.

Mure H, Hirano S, Tang CC, Isaias IU, Antonini A, Ma Y, et al. Parkinson's disease tremor-related metabolic network: characterization, progression, and treatment effects. Neuroimage 2011; 54: 1244–53.

Nagaoka T, Katayama Y, Kano T, Kobayashi K, Oshima H, Fukaya C, et al. Changes in glucose metabolism in cerebral cortex and cerebellum correlate with tremor and rigidity control by subthalamic nucleus stimulation in Parkinson's disease: a positron emission tomography study. Neuromodulation 2007; 10: 206–15.

Payoux P, Remy P, Damier P, Miloudi M, Loubinoux I, Pidoux B, et al. Subthalamic nucleus stimulation reduces abnormal motor cortical overactivity in Parkinson disease. Arch Neurol 2004; 61: 1307–13.

Penny WD, Stephan KE, Daunizeau J, Rosa MJ, Friston KJ, Schofield TM, et al. Comparing families of dynamic causal models. PLoS Comput Biol 2010; 6: e1000709.

Perlmutter JS, Mink JW. Deep brain stimulation. Annu Rev Neurosci 2006; 29: 229–57.

Reis C, Sharott A, Magill PJ, van Wijk B, Parr T, Zeidman P, et al. Thalamocortical dynamics underlying spontaneous transitions in beta power in Parkinsonism. Neuroimage. 2019; 193: 103–14.

Rigoux L, Stephan KE, Friston KJ, Daunizeau J. Bayesian model selection for group studies—revisited. Neuroimage. 2013; 84: 971–85.

Sestini S, Scotto di Luzio A, Ammannati F, De Cristofaro MTR, Passeri A, Martini S, et al. Changes in regional cerebral blood flow caused by deep-brain stimulation of the subthalamic nucleus in Parkinson's disease. J Nucl Med 2002; 43: 725–32.

Stephan KE, Penny WD, Daunizeau J, Moran RJ, Friston KJ. Bayesian model selection for group studies. Neuroimage 2009; 46: 1004–17.

Tanei T, Kajita Y, Nihashi T, Kaneoke Y, Takebayashi S, Nakatsubo D, et al. Changes in regional blood flow induced by unilateral subthalamic nucleus stimulation in patients with Parkinson's disease. Neurol Med Chir (Tokyo) 2009; 49: 507–13.

Tziortzi AC, Haber SN, Searle GE, Tsoumpas C, Long CJ, Shotbolt P, et al. Connectivity-based functional analysis of dopamine release in the striatum using diffusion-weighted MRI and positron emission tomography. Cereb Cortex 2014; 24: 1165–77.

Vafaee MS, ØStergaard K, Sunde N, Gjedde A, Dupont E, Cumming P. Focal changes of oxygen consumption in cerebral cortex of patients with Parkinson's disease during subthalamic stimulation. Neuroimage 2004; 22: 966–74.

Vedam-Mai V, van Battum EY, Kamphuis W, Feenstra MGP, Denys D, Reynolds BA, et al. Deep brain stimulation and the role of astrocytes. Mol Psychiatry 2012; 17: 124–31.

Volonté MA, Garibotto V, Spagnolo F, Panzacchi A, Picozzi P, Franzin A, et al. Changes in brain glucose metabolism in subthalamic nucleus deep brain stimulation for advanced Parkinson's disease. Parkinsonism Relat Disord 2012; 18: 770–4.

Wang J, Ma Y, Huang Z, Sun B, Guan Y, Zuo C. Modulation of metabolic brain function by bilateral subthalamic nucleus stimulation in the treatment of Parkinson's disease. J Neurol 2010; 257: 72–8.

Welter M-L, Houeto J-L, Bonnet A-M, Bejjani P-B, Mesnage V, Dormont D, et al. Effects of high-frequency stimulation on subthalamic neuronal activity in parkinsonian patients. Arch Neurol 2004; 61: 89–96.

Wu DH, Lewin JS, Duerk JL. Inadequacy of motion correction algorithms in functional MRI: role of susceptibility-induced artifacts. J Magn Reson Imaging 1997; 7: 365–70.

Zrinzo L, Yoshida F, Hariz MI, Thornton J, Foltynie T, Yousry TA, et al. Clinical safety of brain magnetic resonance imaging with implanted deep brain stimulation hardware: large case series and review of the literature. World Neurosurg 2011; 76: 164–72.